Table I
Magellanic Plane

	M_V	A deg	$r_\odot$ kpc	r_c pc	PA deg	σ km/s	RV_{obs} km/s	$RV_\odot$ (231)	$RV_\odot$ (300)	Δv_r km/s	Δv_ϕ km/s	FM
Ursa Minor	-8.5	24	63	290	26	7.5	-248	-161	-208	22	18	1.0
Draco	-8.6	11	75	200	8	9.2	-289	-193	-250	20	17	1.0
Sextans	-9.1	18	85	410	18	6.2	224	152	198	19	15	0.8
Carina	-9.3	6	91	230	15	6.8	230	214	277	19	14	1.5
Leo II	-9.9	17	220	190	24	6.7	70	55	72	12	6	0.1
Sculptor	-11.1	3	79	130	33	6.8	107	32	40	20	16	1.9
Leo I	-11.3	24	224	220	44	-	285	108	141	12	6	8.3
Fornax	-12.4	13	138	550	76	11.0	55	88	112	15	9	2.3
SMC	-16.1	21	60	-	-	-	151	140	181	24	22	0.7
LMC	-18.2	6	50	-	-	-	250	192	249	26	26	0.0

The dwarf spheroidals are divided into two groups, 5 feint & 3 bright. Sources: M_V - Mateo 1991, $r_\odot$ & RV_{meas} Kochanek 1996, r_c (core radius) & PA - Irwin & Hatzidimitriou 1993, σ (mean line of sight dispersion) - Milgrom 1995.

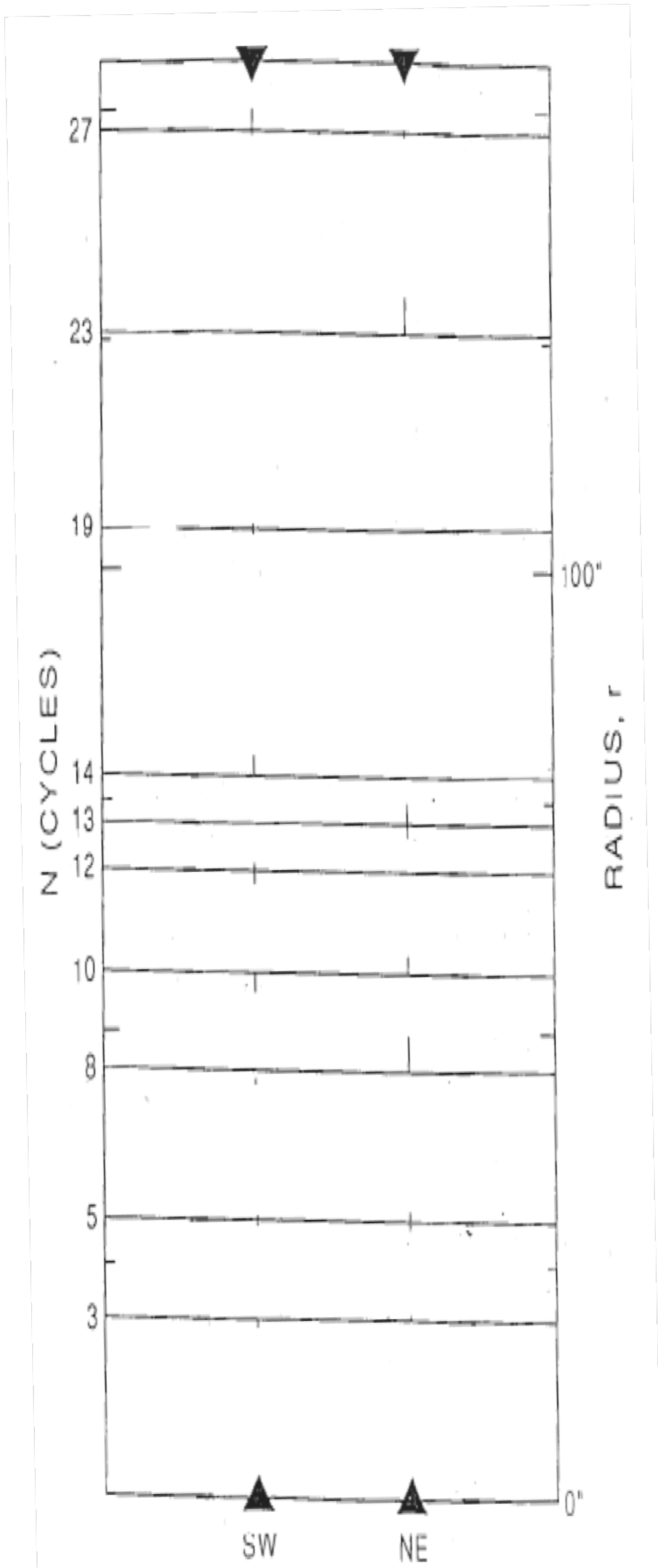

FIG 1. Galaxy NGC 3923. Prieur's measurement[a] of maximum of shell radii vs fitted N of cycle using $r_N = (N + \phi_o)r_o$; $\phi_o = 5/8$ cycle; $r_o = 5.34$"

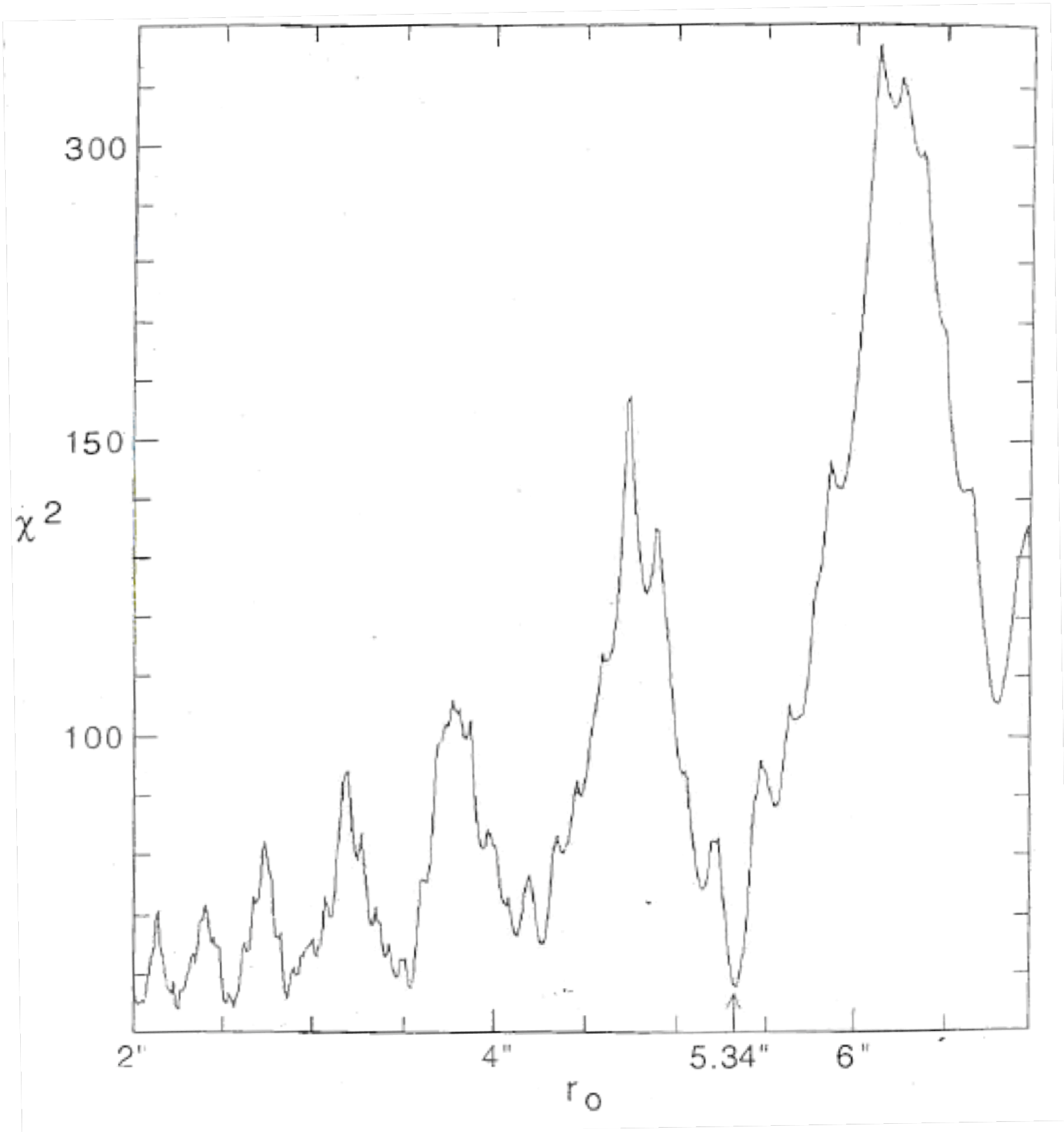

FIG 2. NGC 3923. χ^2 vs r_o for a fixed ϕ_o=5/8 cycle.

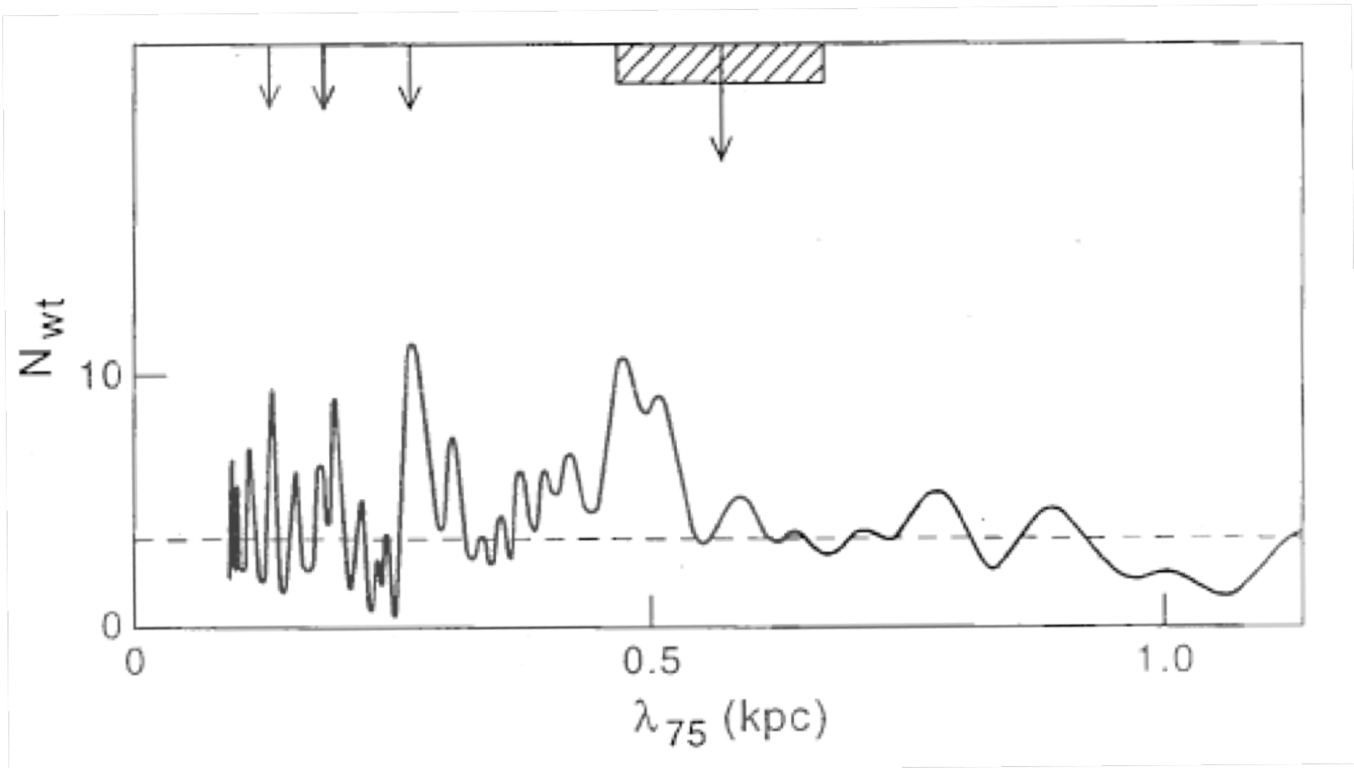

FIG 3. Periodicity of Lens Radii. N_{wt} vs $\lambda_o 75$. The scale for the abscissa has been multiplied by 2/3 from that obtained directly from Kormendy's data. This corrects for the fact that he assumed a Hubble constant of 50 km/s/Mpc rather than the 75 assumed here. The cross-hatched interval is the value of λ_o as determined by the elliptical NGC 3923 using either Prieur's or Tully's estimate of the distance to that galaxy. The arrows at smaller wavelengths mark where expected harmonics of 560 pc should occur.

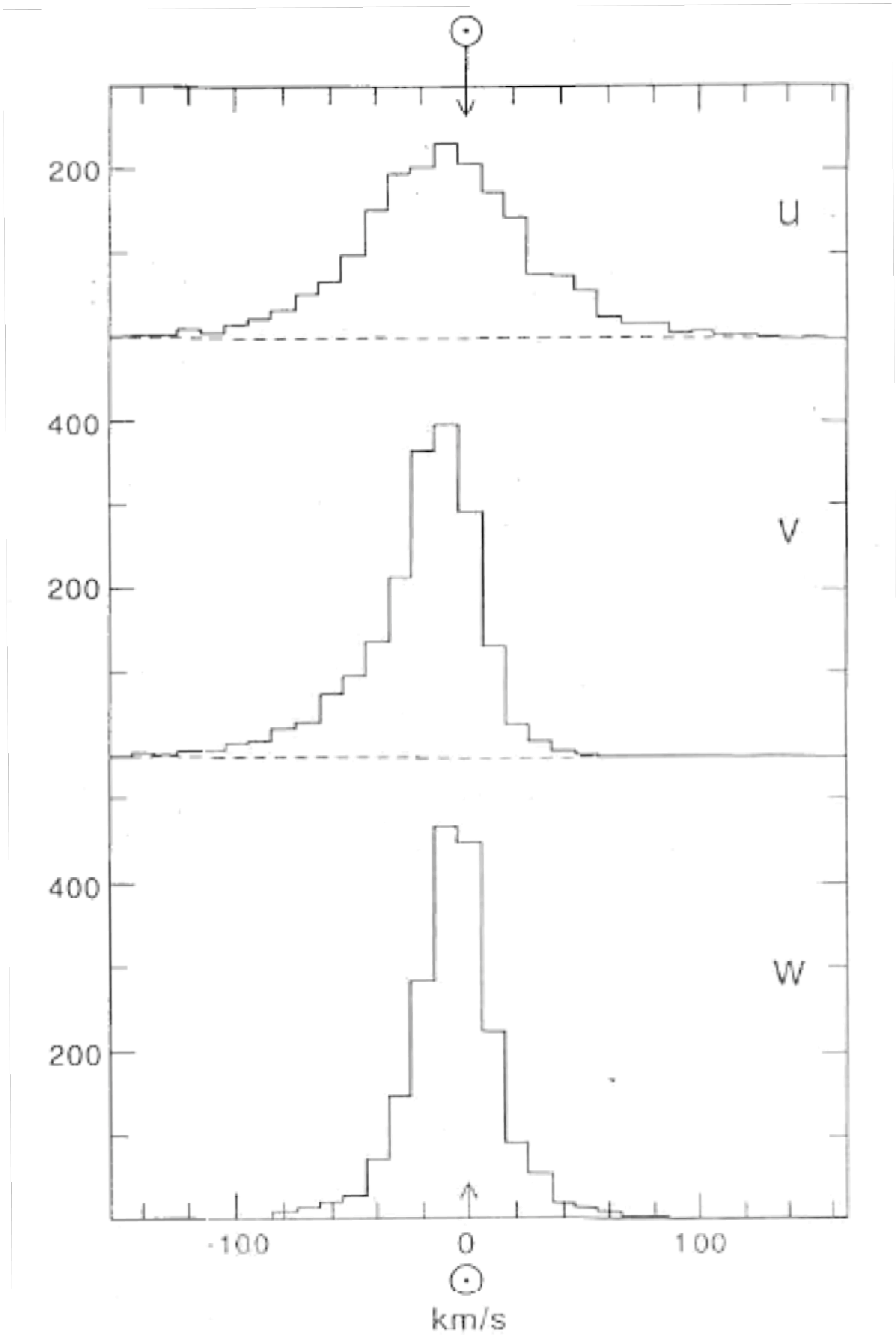

FIG 4. Number of stars in 10 km/s intervals for 1946 stars in CNS3R. Radial, azimuthal, and z-velocities wrt galactic center are -u, v, and w respectively.

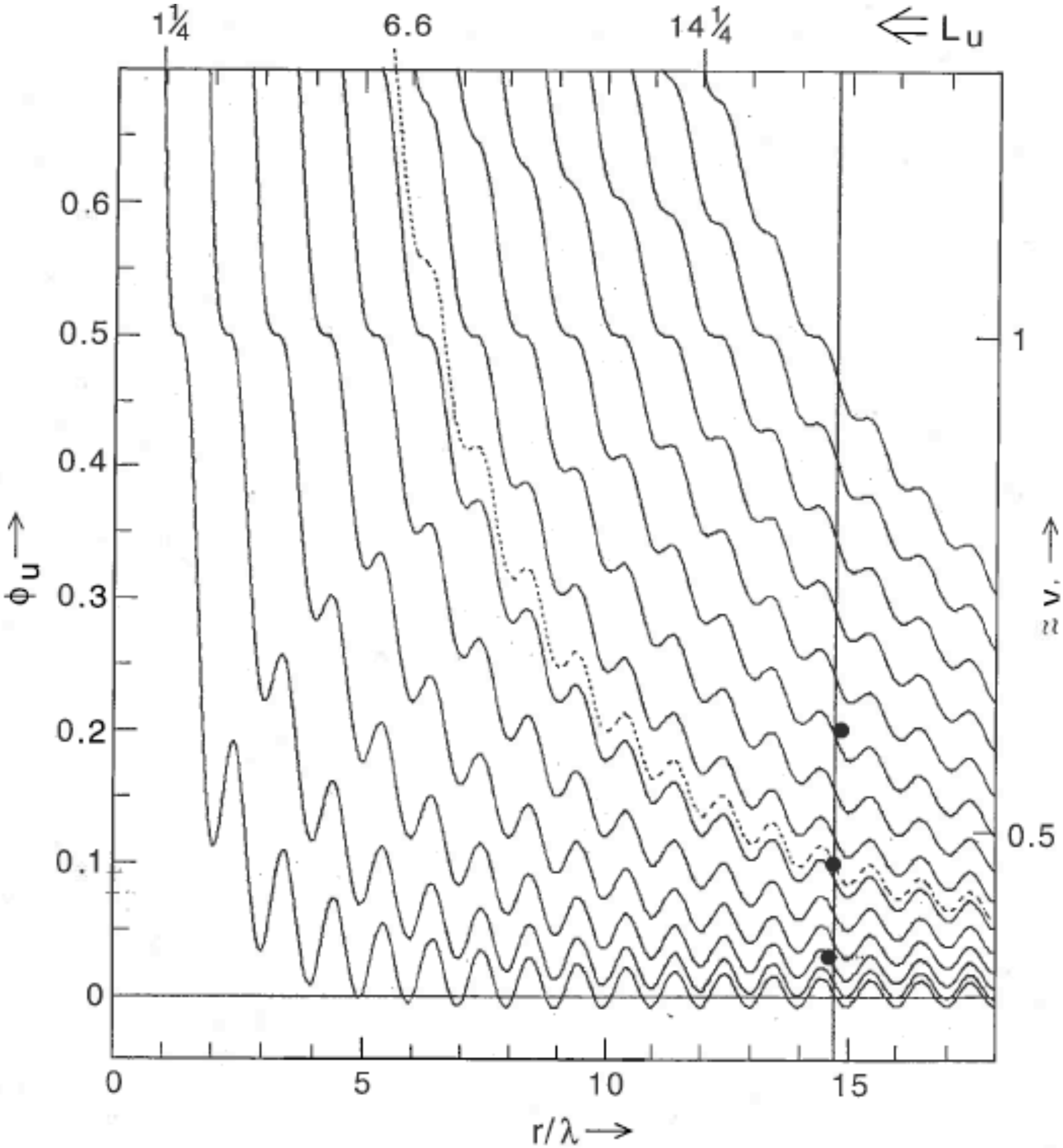

FIG 5. Normalized effective one-dimensional potential ϕ_u vs radius in cycles r/λ_o. Curves given for normalized angular momenta $L_u = 1.25, 2.2514.25$. Also shown are possible positions for the sun assuming for $(v_{escape}, v_{\odot})$: Top dot - (460,300); center dot (680,300) or (510,231); bottom dot - (1200,300)(Non-spherical potential; escape velocity out of plane of disk assumed to 600 km/s).

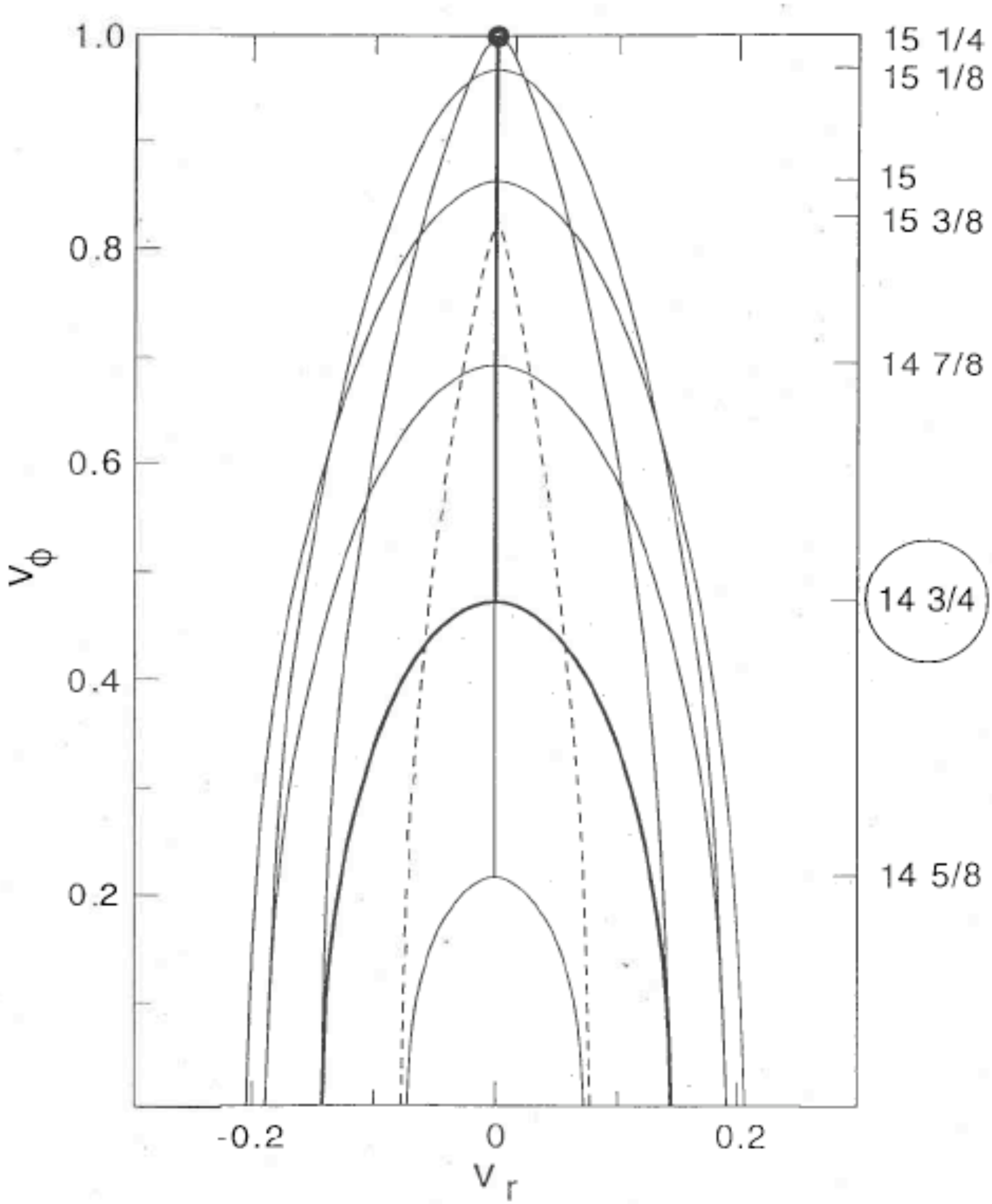

FIG 6. Envelopes of permissible azimuthal velocities v_ϕ vs radial velocity v_r for seven r/λ_o between 14 5/8 and 15 3/8. Permissible velocities are under envelopes. Solid Curves have vertices at inner turning points; dashed at outer. Bold curve corresponds to possible radius for the sun. All velocities normalized to global escape velocity $v_\phi(max)$.

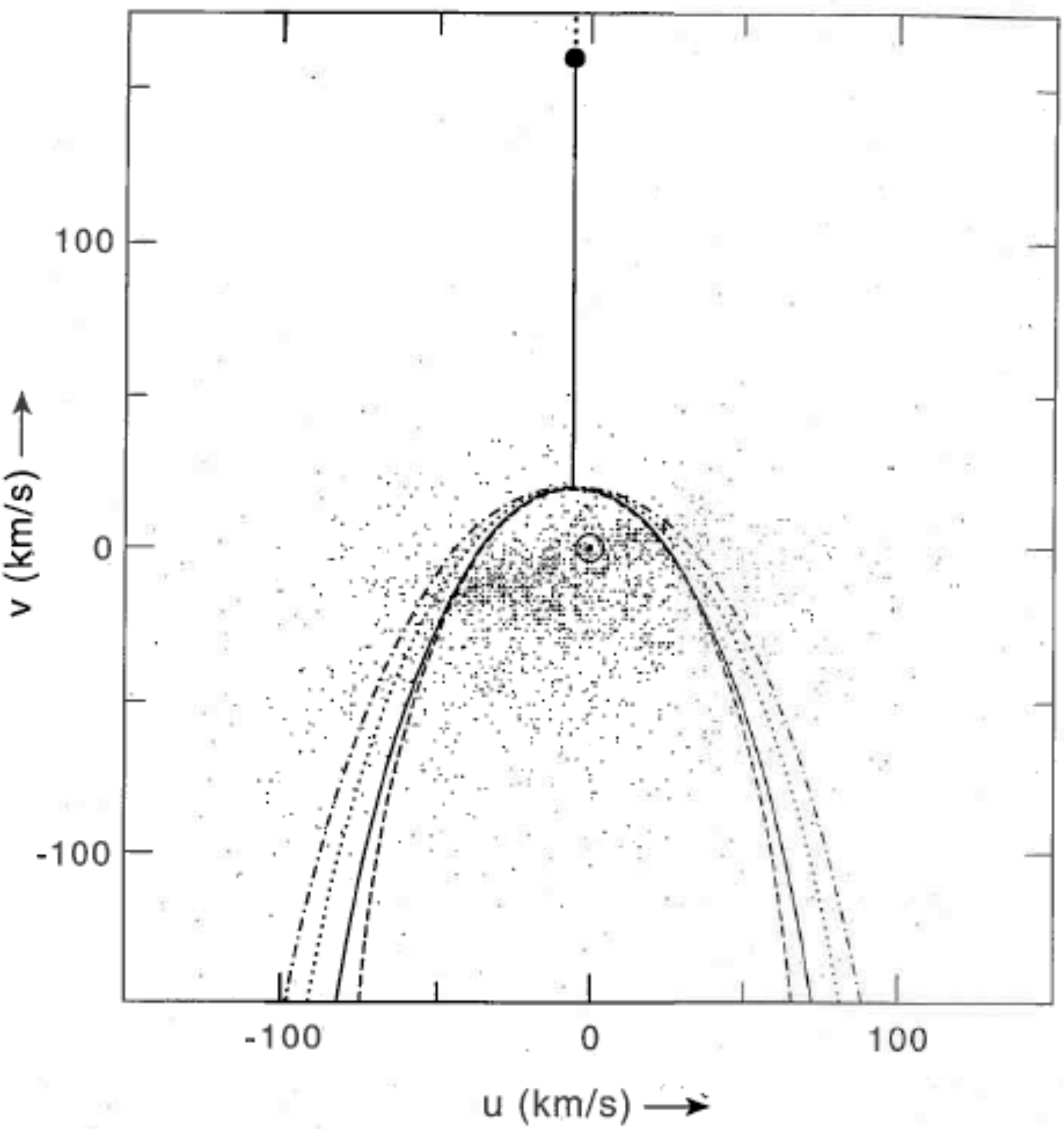

FIG 7. Scatter diagram of u and v velocities of stars in CNS3R. Curves are envelopes expected for different combinations of $(v_{escape}, v_{\odot})$: Solid (460,300), Dash (510,231), Dot (680, 300), Dot-Dash(1200,300) (Noncentral potential).

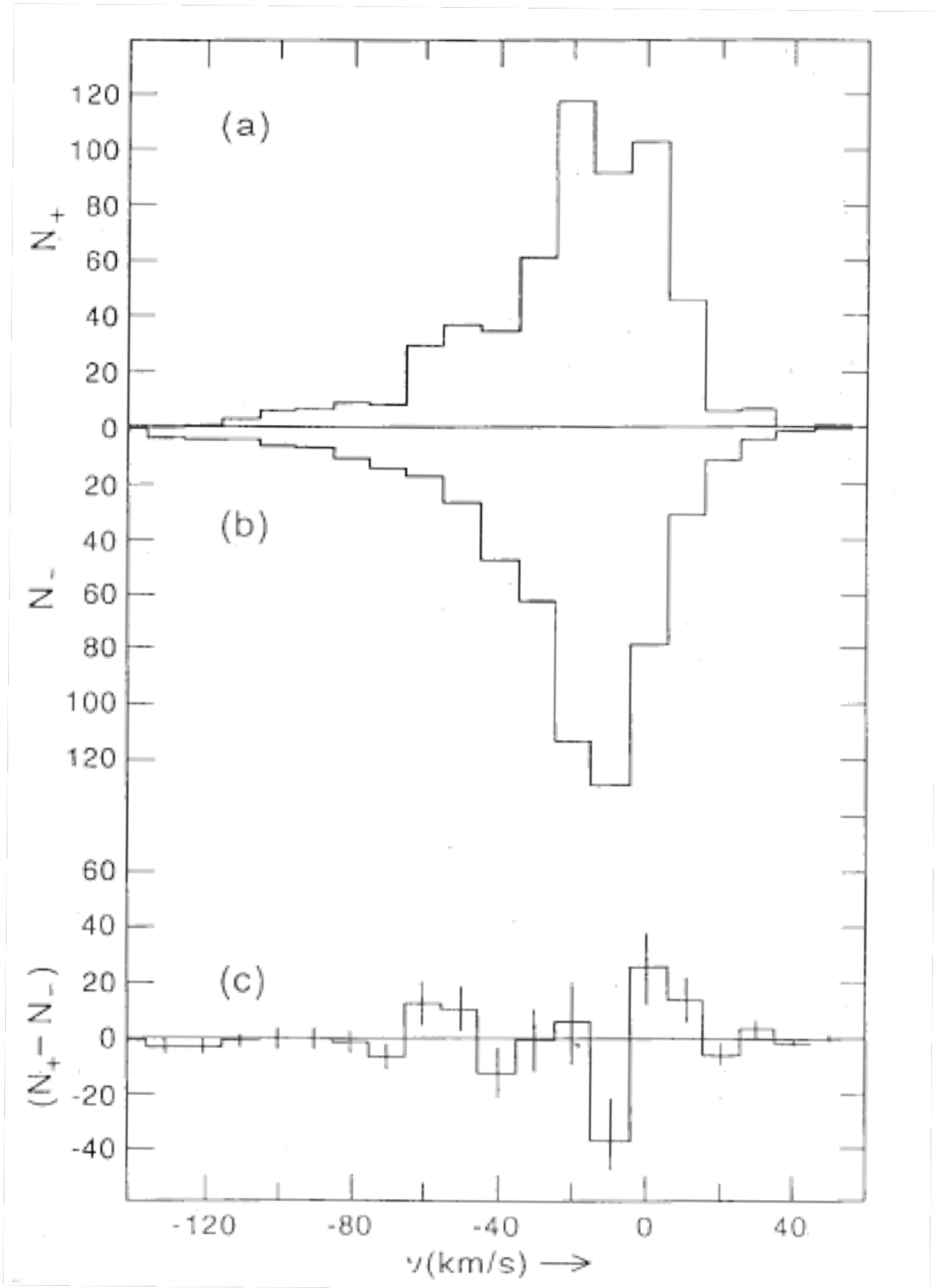

FIG 8. Differential histograms of azimuthal velocities v. (a) N_+ stars more than 6 pc further away from center of galaxy than sun. (b) N_- stars more than 6 pc closer to center of galaxy than sun. (c) $N_+ - N_-$.

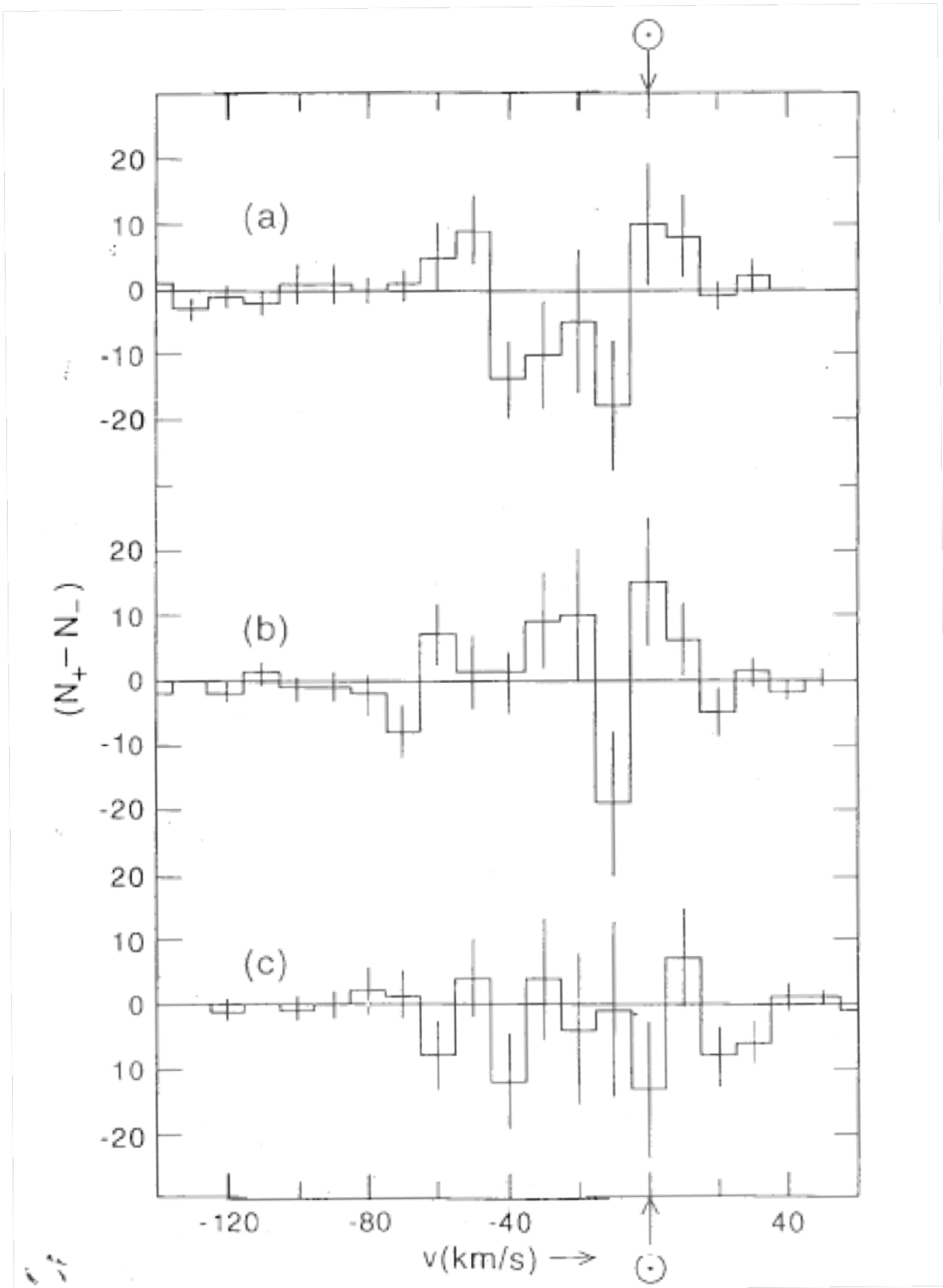

FIG 9. Differential histograms, $N_+ - N_-$. (a) For stars $|r_{star} - r_{sun}| > 12$ pc; (b) 6 pc $< |r_{star} - r_{sun}| < 12$ pc and (c) $|r_{star} - r_{sun}| < 6$ pc.

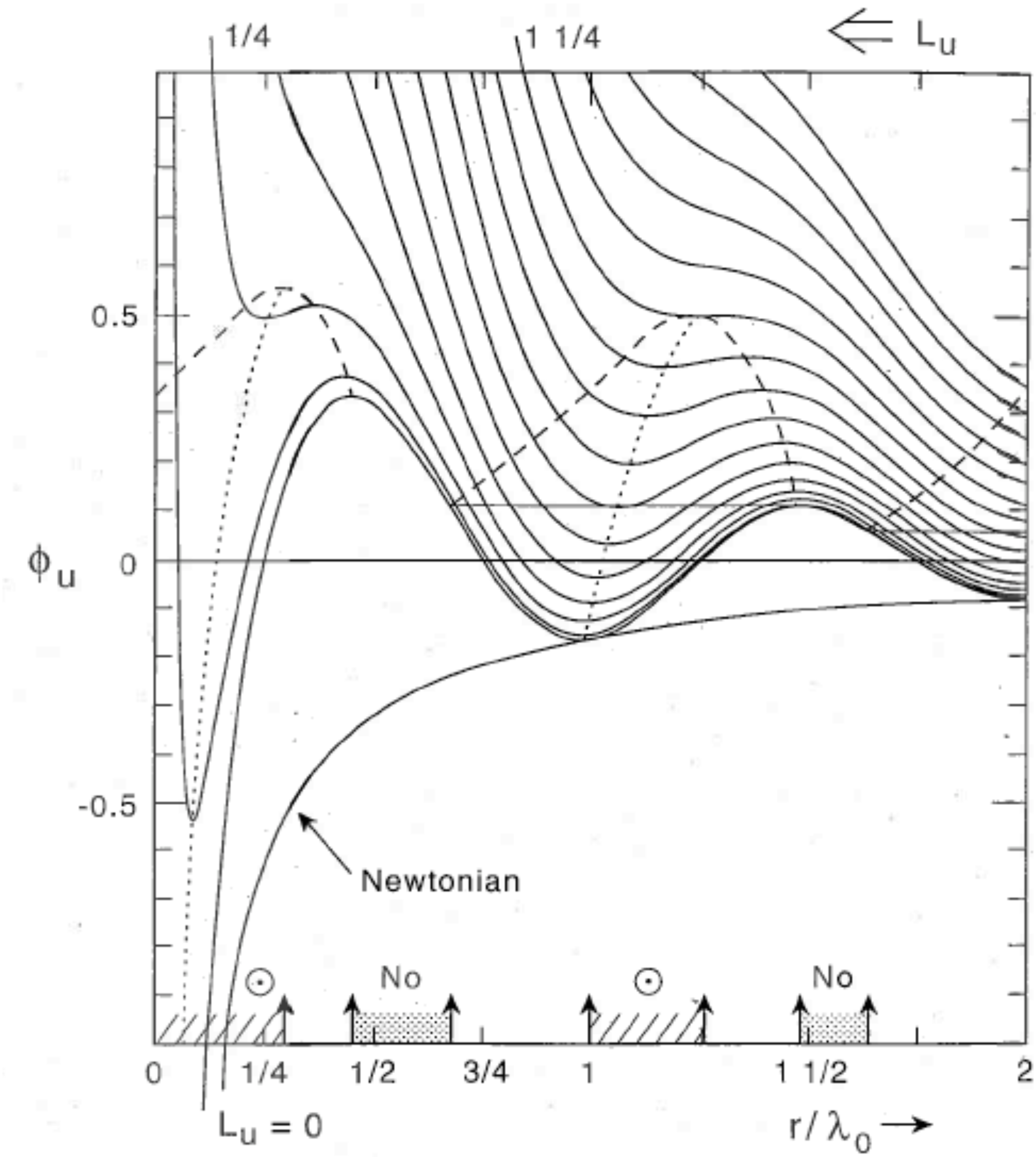

FIG 10. Potential close to a point source mass. Circular orbits allowed only in regions marked ⊙. No bound orbits allowed in regions marked “No”. Unmarked intervals can have radially confined, but non-circular orbits.

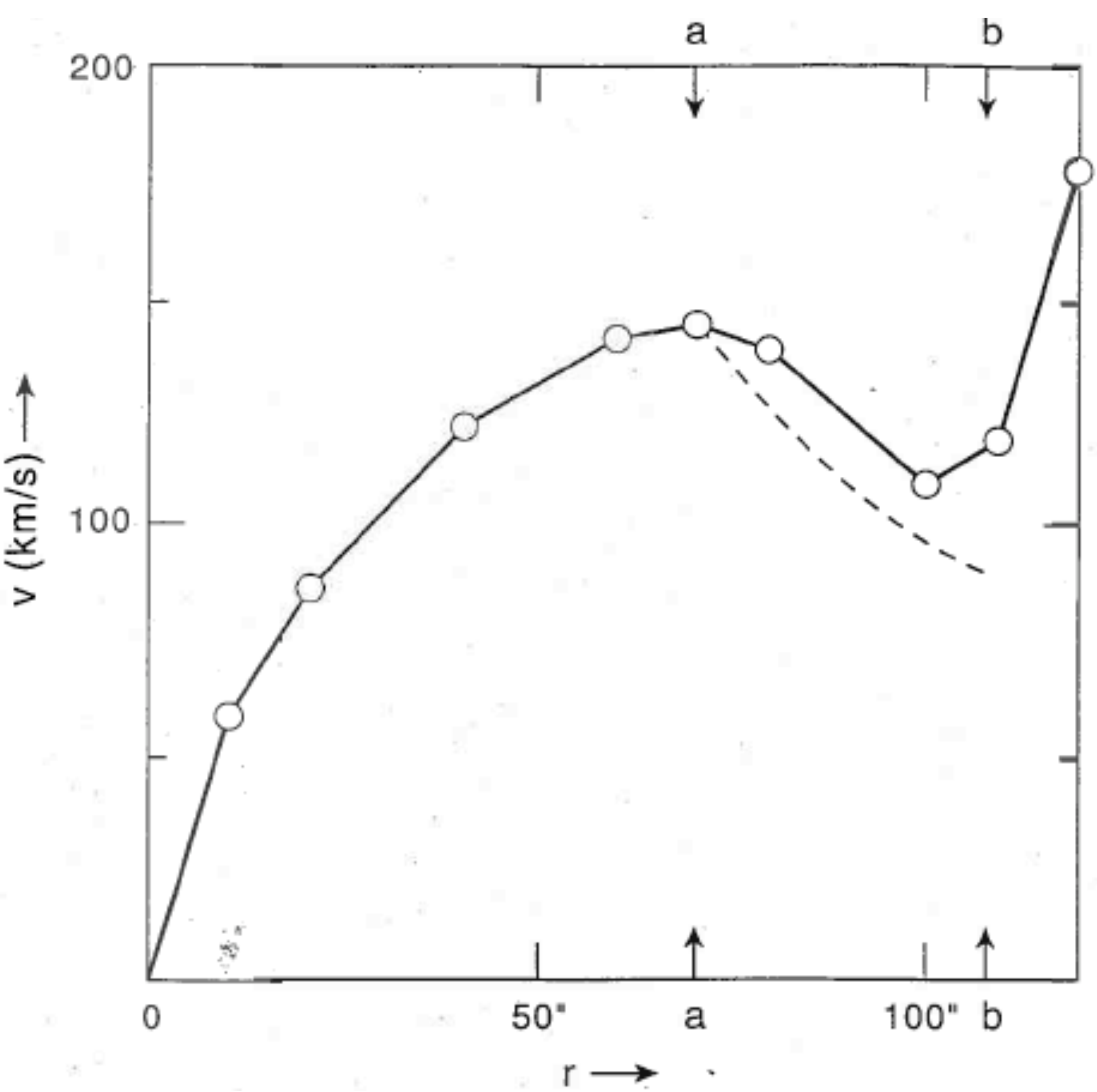

Fig 11. Circular velocity vs radius for M31 (from Table in Rubin & Ford). Markers a (250 pc) and b (380 pc) show limits of first forbidden region. Dashed curve: $1/r$ falloff expected by angular momentum conservation for matter which escapes from radius a.

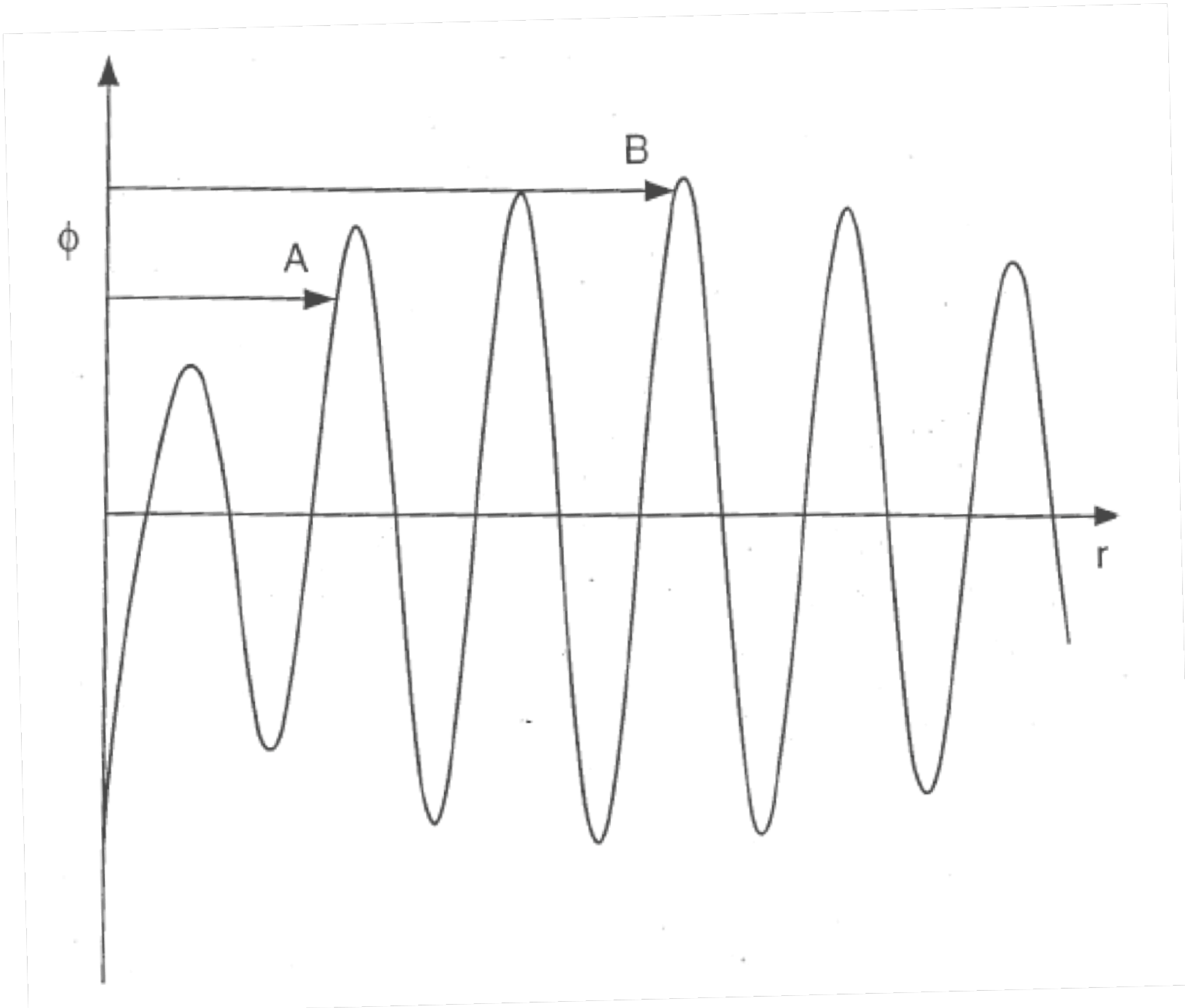

FIG 12. Potential close to an extended source. Bound stars having radial amplitudes $> \lambda_o$ confined to $r < r_B$. Orbits more likely to stop at $r = r_A$.

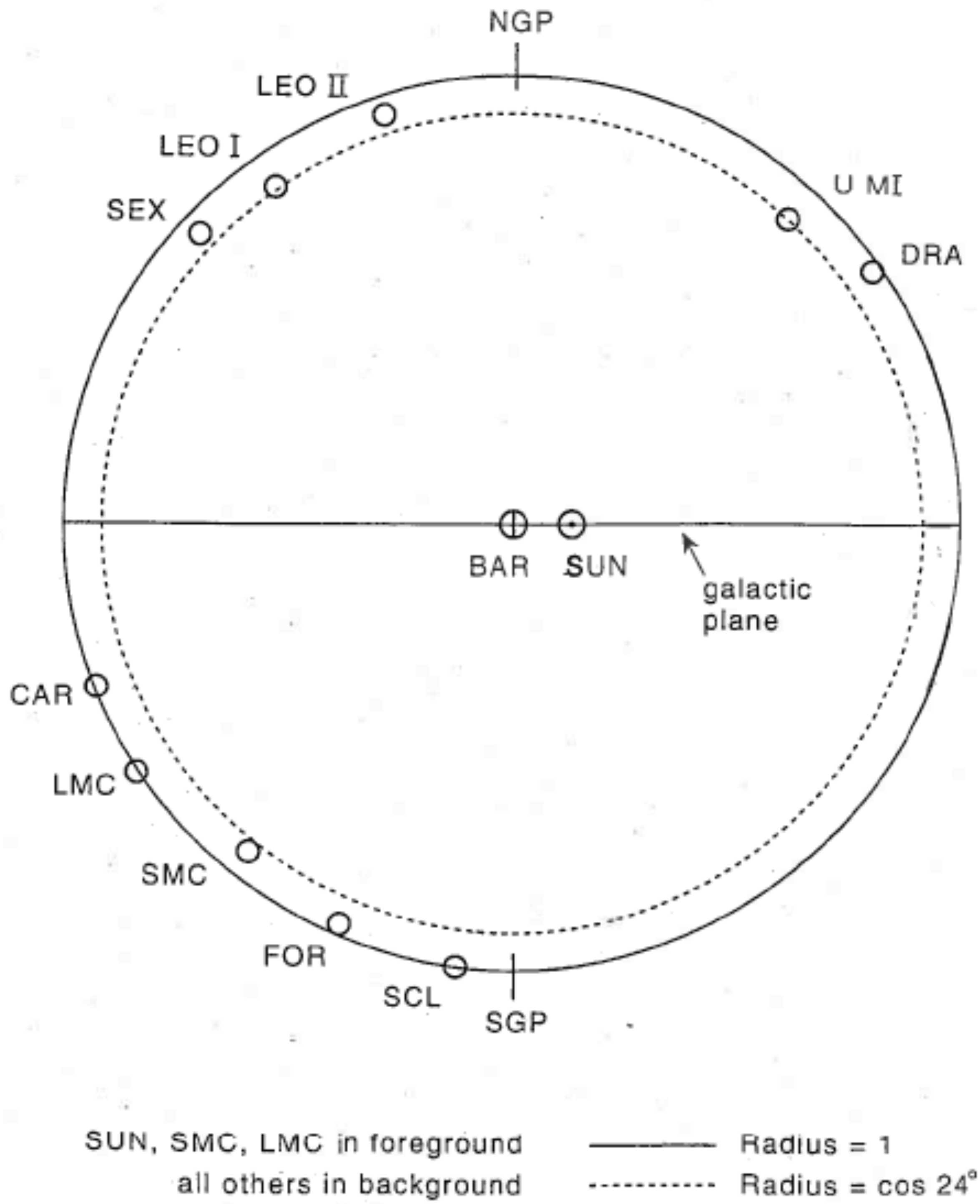

FIG 13. Magellanic Plane shown as a projection of a celestial sphere viewed along the axis of the central bar.

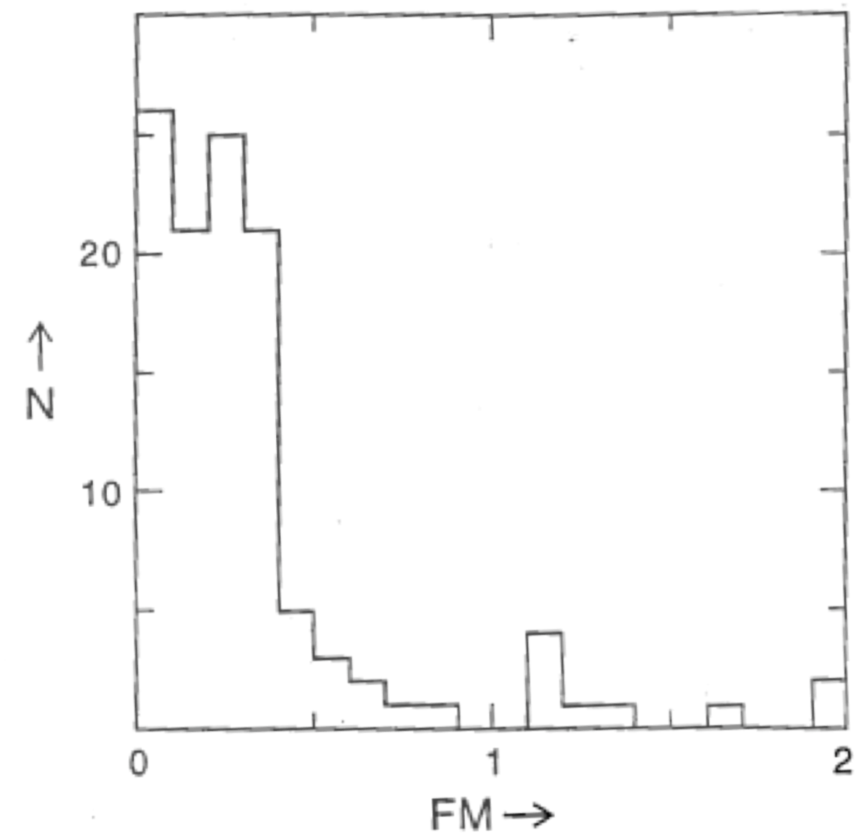

FIG 14. Globular Clusters. Histogram of Number vs Figure of Merit, FM. Clusters having $FM > 1$ in ascending order: Pal 15, AM-1, Rup 106, Pal 2, Pal 3, NGC 5694, Pal 1, Pal 14, Eridanus.

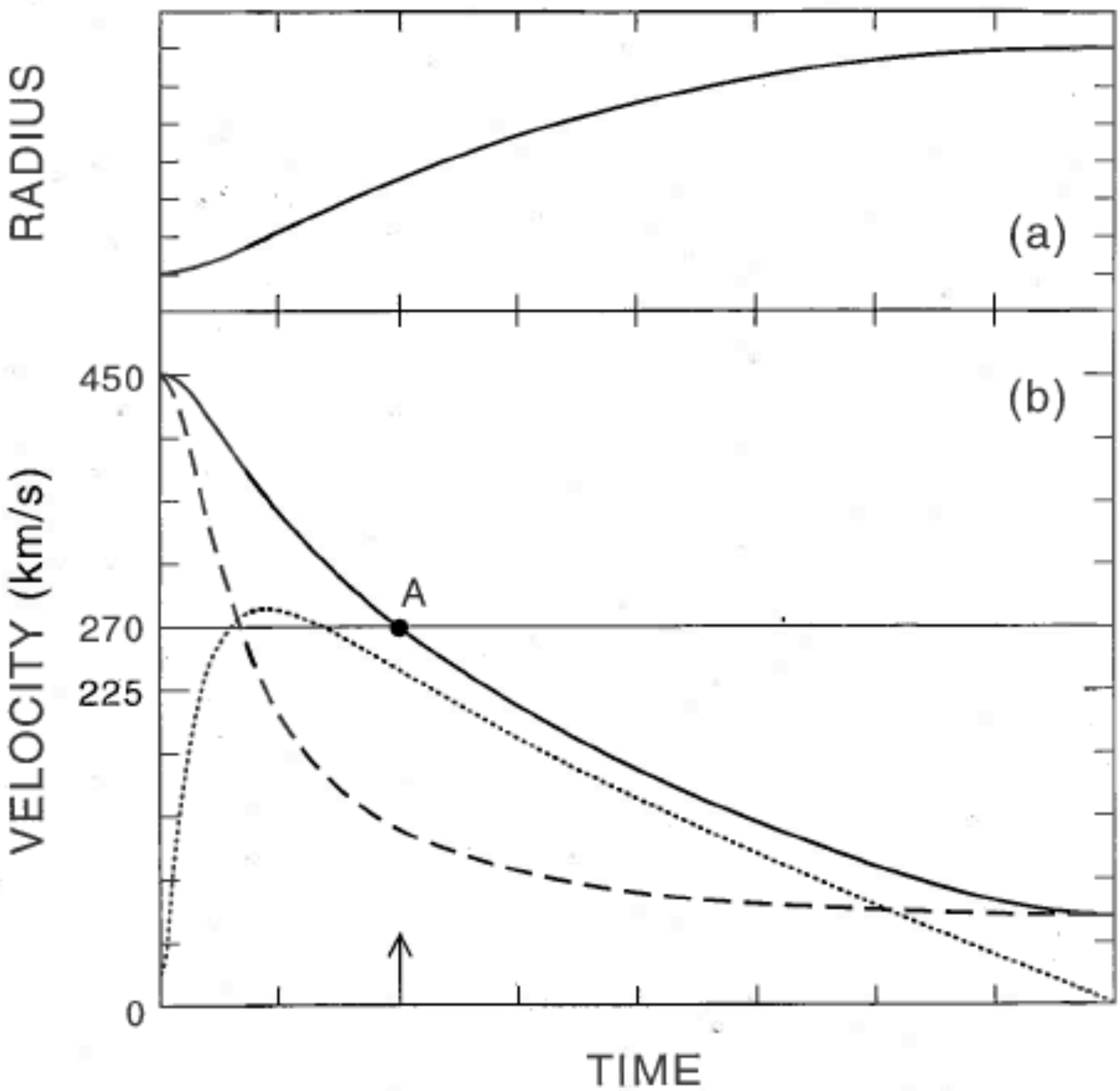

FIG 15. Typical globular cluster in a field $g_r \propto 1/r$. Average $v = 225$ km/s. Solid curve: speed, Dotted: v_r, Dashed: v_θ.

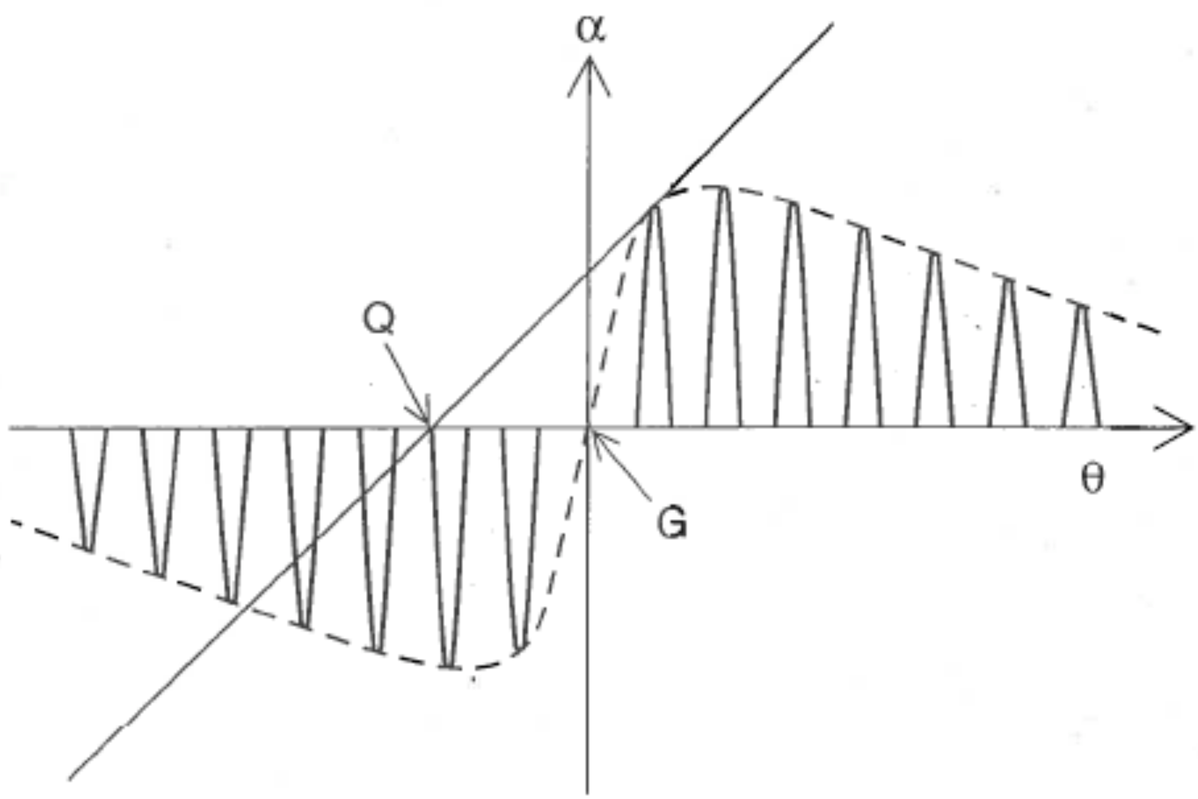

FIG 16. Deflection angle α vs. Image displacement angle θ for light from a quasar Q not quite on axis of intervening galaxy. Image occurs whenever line intersects solid curve. Since magnification is inversely proportional to angle between curve and line, only detectable images are a points of tangency, as illustrated for positive θ.

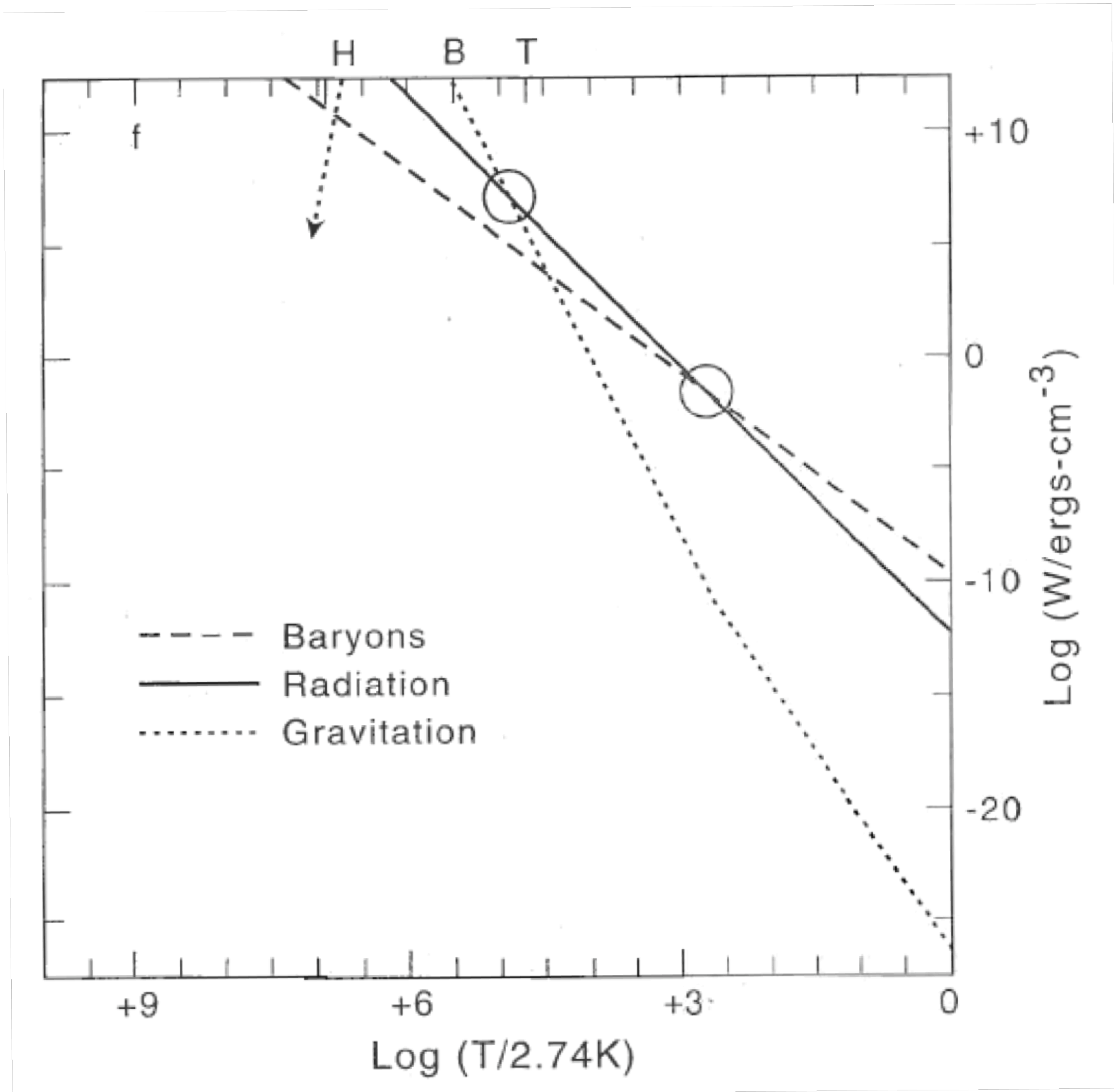

Fig. 17. Mean energy density of universe W vs radiation temperature $T =$ 2.76K $(1+z)$. 0 = present. Gravitational energy dominates before the early circle; after late circle mass dominates. Characteristic temperatures indicated. f: fusion of deuterium and light elements, H: $\lambda_o H_o = 2.76\text{K}\ /T$, B: 128 Mpc $\times 2.76\text{K}\ /T = \lambda_o$.